

Fragile electronic superconductivity in a Bi single crystal

Anil Kumar ¹, Om Prakash ^{2,*}, Rajendra Loke ¹, Arindam Pramanik ³, Rajdeep Sensarma ³, Sitaram Ramakrishnan ⁴,
Biplab Bag ⁵, Arumugam Thamizhavel ¹ and Srinivasan Ramakrishnan ^{6,†}

¹Department of Condensed Matter Physics and Materials Science, Tata Institute of Fundamental Research, Mumbai 400005, India

²Department of Physics and Astrophysics, University of Delhi, Delhi 110007, India

³Department of Theoretical Physics, Tata Institute of Fundamental Research, Mumbai 400005, India

⁴Department of Quantum Matter, AdSE, Hiroshima University, Higashi-Hiroshima 739-8530, Japan

⁵Amity Institute of Applied Sciences, Amity University Jharkhand, Ranchi 834002, India

⁶Department of Physics, Indian Institute of Science Education and Research, Pune 411008, India



(Received 25 January 2023; revised 17 November 2023; accepted 20 November 2023; published 18 December 2023)

It was presumed that semimetallic bismuth (Bi) would not show superconductivity (SC) even at ultralow temperatures (<10 mK) due to its very low carrier density ($\approx 3 \times 10^{17}$ cm⁻³). Recently, we have established bulk superconductivity in an ultrapure (99.9999%) Bi single crystal at $T_c = 0.53$ mK with an extrapolated upper critical field $H_c(0) = 5.2$ μ T measured along the [0001] (trigonal) crystallographic direction [O. Prakash *et al.*, *Science* **355**, 52 (2017)]. At very low concentrations of the charge carriers, we are dealing with fragile Cooper pairs with an estimated large coherence length $\xi_{GL}(0) \approx 96$ μ m. We also stated that one needs to go beyond the conventional electron-phonon coupling (BCS-like) mechanism to understand the SC state in Bi. Bi is a compensated semimetal with electrons and holes as charge carriers. In order to find the charge carriers responsible for the SC, we report the temperature dependence of the anisotropic critical field along the $H \parallel [01\bar{1}0]$ (bisectrix) crystallographic direction and compare it with the earlier data from measurements along the $H \parallel [0001]$ (trigonal) axis. Our theoretical analysis of the critical field anisotropy suggests that the light electrons in the three pockets of the Bi Fermi surface are responsible for the SC, which indicates that Bi is an extremely weak type-II (close to type-I) superconductor. Finally, we present a brief review of the current theories proposed to explain the SC in Bi.

DOI: [10.1103/PhysRevB.108.224512](https://doi.org/10.1103/PhysRevB.108.224512)

I. INTRODUCTION

Although semimetallic Bi has been studied for more than a century, it still draws attention from both theorists and experimentalists who are working in the frontier areas of condensed matter research [1]. Bismuth, which has an electronic configuration ([Xe] $4f^{14} 5d^{10} 6s^2 6p^3$), crystallizes in a distorted rhombohedral structure with the space group $R\bar{3}m$ (No. 166) and lattice constants $a = 4.538$ \AA and $c = 11.823$ \AA . The unit cell consists of two pentavalent Bi atoms, giving rise to a Fermi surface (FS) comprising four ellipsoidal-shaped pockets—three electron pockets and one hole pocket—making Bi a nearly charge compensated semimetal. These pockets account for a very small ($\approx 10^{-5}$) area of the FS, resulting in a carrier density of $n \approx p \approx 3 \times 10^{17}$ /cm³ and a small density of states at FS: $g(E_F) \approx 4.2 \times 10^{-6}$ /(eV atom) [see Figs. 2–4 in the Supplemental Material (SM) [2]]. The low carrier density translates to a single charge carrier shared by nearly 10^5 Bi atoms. This led to a presumption that, if at all, superconductivity in bulk Bi would occur only at ultralow temperatures. Indeed, in 2016 [7], studying a high-purity (6N) single crystal of Bi, some

of us established superconductivity below $T_c = 0.53$ mK with an estimated upper critical field of $H_c(0) = 5.16$ μ T along the $H \parallel [0001]$ crystallographic direction.

Extensive studies on the charge carriers have established that the electrons in Bi have a small effective mass, $m_{\text{eff}} \approx 0.001m_e$, with significant anisotropy, $m_{\text{eff}}^{B\parallel[1000]}/m_{\text{eff}}^{B\parallel[01\bar{1}0]} \geq 200$, while the holes are relatively heavier, $m_{\text{eff}} \approx 0.07m_e$ and have a relatively small mass anisotropy ≈ 10 [8]. To better understand the nature and possible mechanism of superconductivity (SC) in Bi, we have studied the critical field anisotropy using dc-magnetization measurements. Here, we report measurements of the temperature dependence of the upper critical field in a 6N pure single crystal along the $H \parallel [01\bar{1}0]$ -crystallographic direction and present a comparison with the critical field measured along $H \parallel [0001]$ [7]. Our theoretical analysis of the electronic g factor together with the observed critical field anisotropy suggests that the light electrons are primarily responsible for the SC in Bi.

II. EXPERIMENTAL DETAILS

To study the upper critical field along $[01\bar{1}0]$, a single crystal of $2.1 \times 0.3 \times 0.2$ cm³ size (from the same batch used in Ref. [7] with a residual resistivity ratio $\text{RRR} \geq 500$) was cut along the $[01\bar{1}0]$ crystallographic direction (see Fig. 1 in SM [2] for Laue diffraction). The crystal was push-fitted to

*om.prakash.shukla@icloud.com

†ramky07@gmail.com

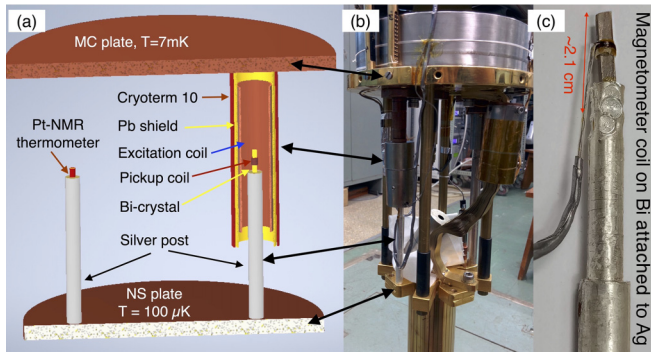


FIG. 1. The schematic drawing of the measurement setup with the magnetic shielding assembly: (a) The overview of the measurement setup consisting of an excitation coil ($B/I \approx 0.04 \mu\text{T}/\mu\text{A}$) enclosed in magnetic shields attached to the MC, Pt-NMR thermometer, and samples mounted on the NS plate ($100 \mu\text{K}$). (b) Actual measurement setup in the dilution fridge. The arrows mark different components shown in the drawing. (c) A Bi single crystal oriented along the $[01\bar{1}0]$ (bisectrix) crystallographic direction is attached to the silver rod. This measurement setup is similar to the thermalization and measurement arrangements reported earlier [7].

an annealed high-purity (5N) silver (Ag) rod with fine Ag powder at the interface to enhance the effective surface contact area [see Fig. 1(c)]. The Ag rod was further pressed onto the crystal to provide better thermal contact and the other end was threaded to the Cu nuclear stage (NS), enabling cooling of the sample down to $T \approx 100 \mu\text{K}$. The dc-magnetization measurement assembly consists of a four-turn magnetometer pickup coil and an excitation coil, both made up of superconducting niobium (Nb) wire. The pickup coil as well as the excitation coil leads were twisted in pairs and enclosed in lead (Pb) foil to minimize coupling to the external magnetic fields and suppress noise in the measurements.

The measurement assembly was enclosed in a magnetic shielding consisting of high permeability material Cryoperm-10, $\mu_r \geq 10^4$ at 4.2 K (SEKELS GmbH, Germany), and superconducting Pb shields and attached to the mixing chamber (MC), a $T = 7 \text{ mK}$ plate of the DRS-1000 dilution fridge (Leiden Cryogenics, Netherlands). This magnetic shielding has shielding factors exceeding 10^6 in both transverse as well as longitudinal directions at the center of the the setup and shields samples from external magnetic fields of the order of $B_{\text{ext}} \approx 10 \text{ mT}$ down to $B_{\text{shielded}} \lesssim 10 \text{ nT}$ [7]. The magnetometer coil is wound directly onto the sample to maximize the filling fraction of the pickup loop and connected to the input coil of a dc superconducting quantum interference device (SQUID) (Tristan Technologies, USA). Figure 1(a) shows a detailed schematic drawing of the measurement setup.

Apart from shielding external magnetic fields, the magnetic shields also decrease the field produced by the enclosed excitation coil. The excitation coil was calibrated while enclosed in the magnetic shielding assembly at 4.2 K using a single-axis magnetometer with a low-field probe (Bartington Instruments Ltd., England) with $\pm 1 \text{ nT}$ resolution to accurately determine the excitation magnetic fields used in the measurements. The pickup coil is connected to the dc SQUID which in turn is connected to the rf amplifier fixed at the head of the cryostat

at room temperature. The rf head is connected to the SQUID control unit which directly reads the output in volts. The dc SQUID output has been calibrated at 4.2 K by measuring the diamagnetic signal from identical sized samples of classical superconductors Nb and Pb. To calibrate the SQUID output voltage with the diamagnetic susceptibility, we used a Rh crystal of the same dimension as the Bi sample and measured the jump in the SQUID output voltage at the SC transition of Rh with different excitation fields. We used similar excitation and pickup coil setups consisting of magnetic shields as mentioned above for calibration [7].

The experiment was carried out in a dilution refrigerator equipped with a single Cu adiabatic nuclear demagnetization stage. The Cu nuclear stage was first cooled by the dilution refrigerator down to 7 mK, followed by magnetization of the Cu nuclear spins by applying a magnetic field of 9 T using a superconducting magnet (Cryogenics, U.K.). The Cu nuclear stage was thermally connected to the mixing chamber using an aluminum (Al) superconducting thermal switch to facilitate isothermal magnetization. The application of a 9 T magnetic field heats up the Cu stage to nearly 40 mK due to the heat of magnetization and we have to wait for nearly 36 h to cool down the magnetized Cu stage to 10 mK. Subsequently, the Al thermal switch is turned off to thermally disconnect the Cu NS from the MC by removing the current in the solenoid enclosing Al switch. A slow adiabatic demagnetization of Cu nuclear spins over a period of 48 h cools down the NS to a base temperature of $100 \mu\text{K}$. Slow demagnetization helps in maintaining thermal equilibrium between the samples, the NS, and thermometers. We used a ^{195}Pt -NMR thermometer for the temperature measurements below 10 mK during adiabatic demagnetization. The NMR thermometer is calibrated against a cerium magnesium nitrate (paramagnetic thermometer) and a SQUID-based noise thermometer (MAGNICON GmbH, Germany) at 10 mK. The SQUID-based noise thermometer can also measure temperatures down to 1 mK and is used along with the NMR thermometer below 10 mK. The details of the adiabatic nuclear refrigerator with temperature measurement and calibration were given in an earlier report [9].

III. RESULTS AND DISCUSSION

A. Magnetization measurements

The zero-field-cooled (ZFC) magnetization measurements in an excitation field of $0.2 \mu\text{T}$ parallel to the $[01\bar{1}0]$ show a sharp jump in the dc SQUID output voltage corresponding to a change in the diamagnetic susceptibility χ_v below 0.53 mK as shown in Fig. 2(a). The $T_c = 0.53 \text{ mK}$ is in agreement with the T_c observed for the field along the trigonal as shown in Fig. 2(b) and matches well with our earlier report [7]. The SC transition is suppressed to lower temperatures with increasing excitation field as shown in Fig. 2(a). All the magnetization measurement curves shown in Fig. 2(a) are in ZFC and recorded during the warmup of the sample. We did not observe any significant difference in the diamagnetic susceptibility between the ZFC and field-cooled (FC) measurements for $H \parallel [01\bar{1}0]$ [see Fig. 2(d) in SM [2]], as was the case for measurements along the $H \parallel [0001]$ [see Fig. 2(a) in Ref. [7]]. The temperature dependences of the critical fields

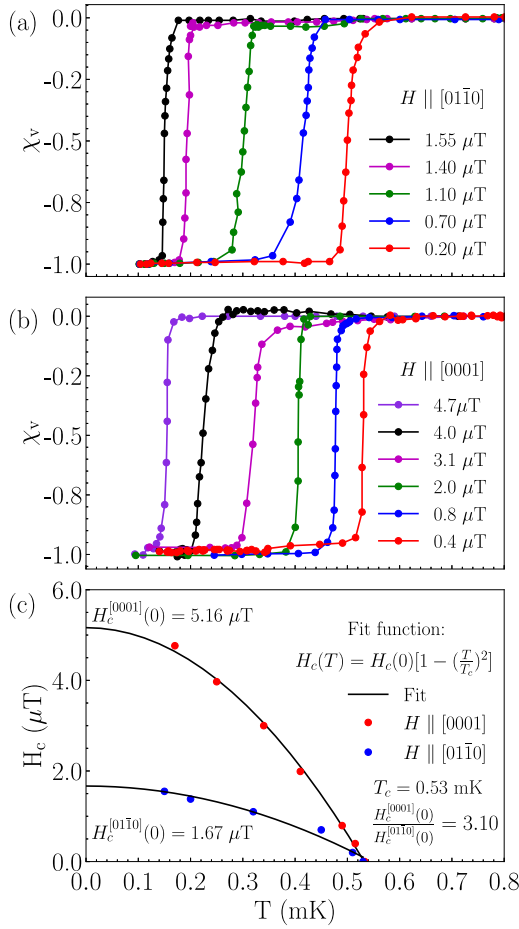


FIG. 2. Diamagnetic susceptibility of the Bi crystal for the field along the $H \parallel [01\bar{1}0]$ (bisectrix) direction in (a) and for the field along the $H \parallel [0001]$ (trigonal) direction in (b). The data for (b) were previously published in Ref. [7] and are presented here for the sake of completeness and comparison. The superconducting transition shifts towards lower temperatures with increasing the applied field. (c) The temperature dependence of the critical fields $H_c(T)$ for the field along the $H \parallel [0001]$ and $H \parallel [01\bar{1}0]$ crystallographic directions.

along the $[01\bar{1}0]$ and $[0001]$ axes are shown in Fig. 2(c). This H - T phase diagram is plotted by taking the transition temperature at a loss of 95% of the diamagnetic susceptibility [at $\chi_v \approx -0.05$ in Fig. 2(a)]. The data are fitted to the function $H_c(T) = H_c(0)[1 - (T/T_c)^2]$, to estimate the value of the critical field at $T = 0$ K. The critical field values along the $[01\bar{1}0]$ and $[0001]$ axes estimated from the fits are 1.67 ± 0.07 and $5.16 \pm 0.07 \mu\text{T}$, respectively, resulting in a critical field anisotropy of $H_c^{[0001]}(0)/H_c^{[01\bar{1}0]}(0) = 3.10 \pm 0.14$.

This critical field anisotropy presents both a challenge and possible window into understanding the mechanism behind the suppression of superconductivity by the magnetic field. If Bi was a strong type-II SC, the anisotropy can be explained in terms of the anisotropic superfluid stiffness of the material inherited from the anisotropic band dispersion of Bi. However, the presence of a sharp jump in the magnetization as shown in Figs. 2(a) and 2(b), and the nearly identical diamagnetic susceptibility in ZFC and FC [7] rules out the possibility. This is not strange given that a majority of elemental

superconductors are type I. Considering Bi as a type-I SC, the critical field H_c is determined by equating the free energy of the superconductor at zero magnetic field with the free energy of the normal state at $H_c(0)$. The anisotropy can then only arise from the dependence of the free energy of the normal state on the direction of the applied field. This free energy is given by $H_c^2/2\mu_0(1 + \chi_v)$, where χ_v is the volume magnetic susceptibility of the material. Even for a strongly diamagnetic material such as Bi with $\chi_v \approx 10^{-4}$ [10], the anisotropic effects from χ_v can be neglected. Thus, it is hard to explain an anisotropic factor of 3.26 in terms of $H_c(0)$. Additionally, a simple estimate of $H_c(0)$, assuming an energy gap $\Delta(0) = 1.764k_B T_c$ [7] with $T_c = 0.53$ mK and the pairing of electrons with the density of states (per pocket per spin) at the Fermi level $N_0^g = 9.2 \times 10^{18} \text{ eV}^{-1} \text{ cm}^{-3}$ [11] leads to an isotropic $H_c(0) = 0.2 \mu\text{T}$, which is much lower than the values observed experimentally. A similarly low value of $H_c(0)$ is obtained if one assumes hole pairing instead of electron pairing. If both electrons and holes participate in the pairing, the estimated $H_c(0) = 0.3 \mu\text{T}$ is still lower than the experimentally measured values as shown in Fig. 2(c).

B. Theoretical calculations of g -factor anisotropy

The anisotropy of the critical field can be understood if one assumes that Bi is a weakly type-II superconductor and the transition is given by the Pauli paramagnetic limit. In this case, we compare the pairing energy gain to the Zeeman energy cost paid by the electrons/holes to maintain similar Fermi surfaces for the two spin components, $g\mu_B H_c = \frac{\Delta(0)}{\sqrt{2}}$ [12]. To further test this, we use the following model Hamiltonian for each of the three electron pockets to extract the anisotropic g factor,

$$H_e(\vec{k}) = [\hbar v_z k_z \sigma^z + \hbar v_\perp (k_x \sigma^x + k_y \sigma^y)] s^x + \Delta_{\text{bg}} s^z, \quad (1)$$

where σ^i 's and s^i 's are the Pauli matrices in the spin and orbital space, respectively. We use $v_z = 6.6 \times 10^4$ m/s, $v_\perp = 8.1 \times 10^5$ m/s, and $\Delta_{\text{bg}} = 7.5$ meV [11]. Here, z denotes the direction along the Γ - L line in the Brillouin zone (BZ), the long axis of the electron pockets. Figure 3 shows the BZ and the electron and hole pockets contributing to the FS. The electron pockets have a tilt angle of 7° with the $[1000]$ - $[01\bar{1}0]$ (binary-bisectrix) plane.

To find the spin splitting in the presence of an external magnetic field, we block diagonalize [8,13] the Hamiltonian in the orbital space to get the effective spin Hamiltonian,

$$H_{\text{spin}} = \frac{\hbar e}{\Delta_{\text{bg}}} v_z v_\perp H_x \sigma^x + \frac{\hbar e}{\Delta_{\text{bg}}} v_z v_\perp H_y \sigma^y + \frac{\hbar e}{\Delta_{\text{bg}}} v_\perp^2 H_z \sigma^z, \quad (2)$$

where $H = (H_x, H_y, H_z)$ is the external magnetic field. This allows us to extract the effective g factors for different electron pockets for H in three different directions, $[0001]$ (trigonal), $[1000]$ (binary), and $[01\bar{1}0]$ (bisectrix) [see Fig. 3(b)], which are listed in Table I and are roughly consistent with estimates from cyclotron resonances [8].

We note that a larger value of g in a particular direction implies a smaller critical field $H_c(0)$ in that direction. From Table I, we note that the g factor along the $[01\bar{1}0]$ direction is larger than the g factor along the $[0001]$ direction, and hence the in-plane critical field along the $[01\bar{1}0]$ should

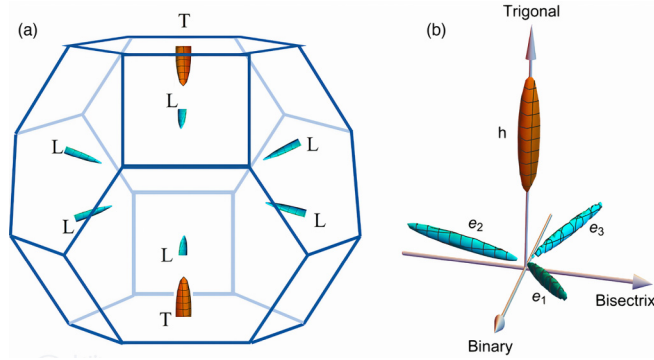


FIG. 3. (a) The first Brillouin zone and the Fermi surface of bismuth. (b) Enlarged electron (blue) and hole (red) pockets. The electron pockets make $\alpha \approx 7^\circ$ tilt angle with the [1000]-[0110] (binary-bisectrix) plane. The pocket e_2 lies along the [0110] direction.

be smaller than the critical field along [0001], in agreement with our observations as shown in Fig. 2(c). Furthermore, the ratio of $H_c(0)$ along [0001] to that along the [0110] is $H_c^{[0001]}(0)/H_c^{[0110]}(0) = g_{[0110]}/g_{[0001]} \approx 3.41$ (from Table I) which agrees well with the anisotropy ratio of ≈ 3.10 measured experimentally [see Fig. 2(c)]. Our individual estimates for $H_c^{[0001]}(0) \approx 3.4 \mu\text{T}$ and $H_c^{[0110]}(0) \approx 1 \mu\text{T}$ are also close to the experimentally observed values [Fig. 2(c)]. We also note that the g factor for the hole pocket is ≈ 63 in the [0001] direction and ≈ 0.8 in the plane [8]. Thus a Pauli limit calculation with the hole pocket would yield a larger in-plane upper critical field compared to the critical field along the [0001] axis contrary to the experimental findings. Thus the anisotropy seen in the experiments strongly points to the pairing of electrons driving superconductivity in Bi.

C. Overview of theoretical models

We now consider the models put forth to explain the observation of SC in Bi. Earlier, Srinivasan *et al.* [14] used a simplified two-band model for describing the longitudinal dielectric function and found that the attractive interaction responsible for the instability of the normal ground state arises not only from the exchange of lattice phonons, but also from the electron-hole sound mode, provided the ratio of the average hole to the electron mass, $m_h/m_e \neq 1$. This condition is easily satisfied in the case of Bi and they estimated the T_c to be around 1 mK. However, so far there is no experimental evidence for the existence of the electron-hole sound (EHS) mode (a soundlike longitudinal collective mode) in Bi.

Another model proposed by Mata-Pinzón *et al.* [15] numerically calculated the electronic and vibrational densities

TABLE I. Calculated g -factor anisotropy of the three electron pockets in Bi.

Pocket	[0001] (trigonal)	[1000] (binary)	[0110] (bisectrix)
e_1	293	1716	1000
e_2	293	162	1979
e_3	293	1716	1000

of states (eDOS and vDOS, respectively) of the crystalline and amorphous forms of Bi. The calculations showed that the eDOS of amorphous Bi (a -Bi) is about $4\times$ larger than that of crystalline Bi (c -Bi) at the Fermi energy, whereas for the vDOS, the energy range of the amorphous is roughly the same as the crystalline even though the actual shapes are quite different. Using the experimental parameters obtained for a -Bi and employing a simple weak-coupling BCS mode, they gave an upper limit of 1.3 mK as the superconducting transition for a pure Bi crystal. Furthermore, they suggested that the electron-phonon coupling (λ) is larger in a -Bi as compared to c -Bi as indicated by the λ obtained via McMillan's formula, $\lambda_c = 0.24$ for c -Bi while experiment and theory suggest $\lambda_a = 2.46$ for a -Bi. Therefore, with respect to the c -Bi, superconductivity in a -Bi is enhanced by the higher values of λ and eDOS at the Fermi energy. Though this model is simple and predicts T_c of the Bi crystal somewhat near to the measured value, use of the electron-phonon mechanism in the formation of Cooper pairs is not justified due to the failure of the Migdal's adiabatic approximation [16] which is central to any electron-phonon coupling scheme including the BCS theory. This is due to the fact that the Fermi energy (25 meV) and lattice energy (15 meV) of crystalline Bi are comparable. We believe that the underlying mechanism for superconductivity in c -Bi is entirely different from that of a -Bi. The mechanism for superconductivity in the latter is due to an electron-phonon interaction which is firmly established.

Let us now look at the other models which suggest unconventional mechanisms [11,17–20] for the observation of superconductivity in Bi. Koley *et al.* [17] suggested that fluctuating excitons could be the glue for superconductivity in Bi. They showed that a two-fluid model composed of preformed and dynamically fluctuating excitons coupled to a tiny number of carriers can provide a unified understanding of the anomalous temperature dependence of the resistivity below 1 K as well as superconductivity in Bi below 1 mK. Our resistivity data in Fig. 4 clearly show a deviation from T^2 dependence of the resistivity below 800 mK and ultimately show a $T^{1.8}$ behavior down to 15 mK. Koley's model has proposed that resonant scattering involving a very low density of renormalized carriers and excitonic liquid drives the logarithmic enhancement of vertex corrections, boosting superconductivity in Bi. The model also explains the temperature dependence of the normal state resistivity down to 15 mK. However, at present it is not clear whether such a model can explain the anisotropy observed in the critical fields.

Bhaskaran [18] suggested that a potentially high- T_c SC from the resonating-valence-bond (RVB) mechanism is lost in Bi. However, some superconducting fluctuations survive and the tiny Fermi pockets are viewed as remnant evanescent Bogoliubov quasiparticles that are responsible for the anomalous normal state. A multiband character admits the possibility of \mathcal{PT} -violating chiral singlet superconductivity Bi. It remains to be seen whether such a chiral superconductor exists and can explain the observed anisotropy. Moreover, Bhaskaran's model also suggests elements such as Sb and As should also exhibit SC at low temperatures. We did not observe SC in single crystals of both of Sb and As down to 0.1 mK in a field of 0.4 μT .

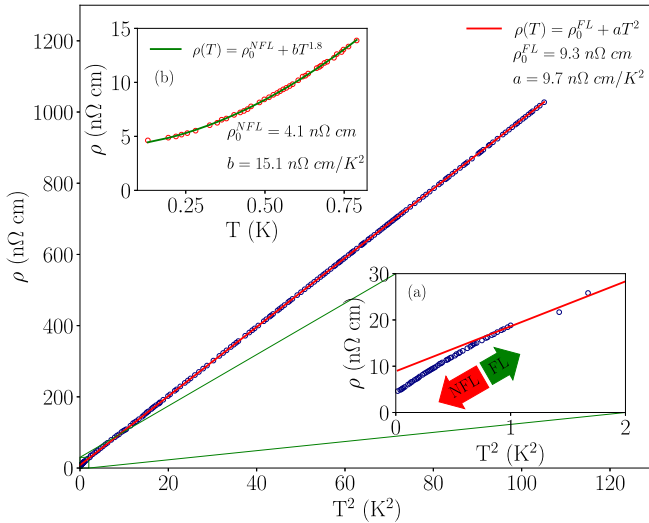


FIG. 4. The low-temperature resistivity in bismuth. (a) The resistivity shows Fermi-liquid behavior down to 800 mK. (b) The Fermi-liquid behavior breaks down below 800 mK and the resistivity is best described by $T^{1.8}$. This suggests that the superconductivity in bismuth emerges out of a non-Fermi-liquid state.

Ruhman and Lee [11] have argued that conventional electron-phonon coupling is too weak to be responsible for the binding of electrons into Cooper pairs. They showed that Bi is the first material to exhibit superconductivity driven by the retardation effects of Coulomb repulsion alone. They claimed that SC of Bi at low carrier concentration arises only due to the long-ranged interactions that are capable of causing such an instability. In the absence of any experimental evidence of a critical point, they investigated the more likely scenario in which the dynamically screened Coulomb repulsion gives rise to an effective retarded attraction on the energy scale of the longitudinal plasma oscillations. Further, they used an approximate isotropic band structure and the random phase approximation for the screened Coulomb interaction. Within these approximations, they found the above-mentioned weak-coupling instability. The transition temperature is greatly enhanced by the existence of a heavy-hole band which has a large mass that allows for an enhancement of the static screening (Thomas-Fermi) without enhancing the plasma frequency. They also showed that T_c is not dramatically decreased when the acoustic plasmon is absent. Therefore, it was concluded that an acoustic plasmon does not contribute to attractive interactions in Bi. They emphasized that the model works only in the s -wave coupling and the scenario might change with higher angular momentum coupling that might result in the SC of bismuth. Our analysis suggests that electrons (not holes) are responsible for SC in Bi and that needs to be reconciled with Ref. [11].

Tewari and Kapoor [19] suggested that the superconductivity of Bi arises due to the electrons belonging to the three pockets. They claimed that the electrons in Bi behave as a rare gas with an interparticle separation of nearly 185 Å. In such a dilute system, the peculiar oscillatory behavior of the generalized electronic dielectric function at large distances can give rise to an attractive interaction between two elec-

trons. This model is valid at extremely low temperatures for a very low-density electron gas, so that there is no electron-phonon interaction and the interaction amongst the electrons can be expressed in terms of a weak two-body potential characterized by a negative scattering length. The dilute nature of the electron gas is a crucial and necessary requirement (i.e., $k_F \times a \ll 1$, where a is the distance between atoms) to observe SC in Bi. We have calculated the Sommerfeld coefficient (γ) using the formula $\gamma = \frac{\pi^2}{3} k_B^2 g(E_F)$, where $g(E_F)$ is the density of carriers at the Fermi level. Here, the carrier comprises both electrons and holes. A simple estimate of γ , assuming the density of states (per pocket per spin) of electrons at the Fermi level, $N_0^e = 9.2 \times 10^{18} \text{ eV}^{-1} \text{ cm}^{-3}$ [11], and the density of states (per spin) of holes at the Fermi level, $N_0^h = 3.5 \times 10^{19} \text{ eV}^{-1} \text{ cm}^{-3}$ [11], gives $\gamma \approx 4 \mu\text{J K}^{-2} \text{ mol}^{-1}$. This estimated value is quite close to the experimentally obtained $\gamma \approx 5 \mu\text{J K}^{-2} \text{ mol}^{-1}$ [7]. Therefore, a refinement of the model proposed by Ref. [19] is required to understand the temperature dependence of the critical field. Finally, the model proposed by Krüger [20] relies on the hypothesis that the nonadiabatic Heisenberg model presents a mechanism of Cooper pair formation generated by the strongly correlated atomiclike motion of the electrons in narrow, roughly half-filled superconducting bands of special symmetry. In this case, the formation of Cooper pairs is not only the result of an attractive electron-electron interaction but is additionally the outcome of quantum mechanical constraining forces. According to his assertion, only these constraining forces operating in superconducting bands may produce eigenstates in which the electrons form Cooper pairs. He argued that both Bi at atmospheric pressure and Bi at 122 GPa have nearly half-filled narrow electronic bands which may be responsible for superconductivity in both these phases of Bi. However, this model does not provide any information on the superconducting properties of Bi apart from the estimation of T_c . It is clear that more theoretical work is required to understand the superconducting properties of this fragile electronic SC of Bi.

IV. SUMMARY AND CONCLUSIONS

In summary, we have studied the superconducting anisotropy in high-quality single crystals of bismuth using dc-magnetization measurements for the magnetic field along the $H \parallel [01\bar{1}0]$ in a magnetically shielded setup. The comparison of the upper critical field $H_c(0)$ along $[0001]$ with those along $[01\bar{1}0]$ results in an anisotropy factor of $H_c^{[0001]}(0)/H_c^{[01\bar{1}0]}(0) \approx 3.10$. Our theoretical calculation of the electronic Lande's g factor along $[0001]$ and $[01\bar{1}0]$ shows an anisotropic factor of 3.41, which is very close to the measured critical field anisotropy, suggesting that in otherwise fully compensated semimetal bismuth with nearly equal number of holes and electrons, the electrons are primarily involved in pair formation.

ACKNOWLEDGMENTS

R.S. and A.P. acknowledge use of computational facilities at the Department of Theoretical Physics. R.S. acknowledges

support from the Department of Atomic Energy, Government of India, under Project Identification No. RTI 4002. R.S.

thanks Pratap Raychaudhuri, Unmesh Ghorai, and Mursalin Islam for useful discussions.

-
- [1] V. S. Édel'man, Electrons in bismuth, *Adv. Phys.* **25**, 555 (1976).
- [2] See Supplemental Material at <http://link.aps.org/supplemental/10.1103/PhysRevB.108.224512> for (Sec. A) crystallographic alignment along [01 $\bar{1}$ 0] using Laue diffraction as shown in Fig. 1; (Sec. B) details of the band structure and ZFC and FC data as shown in Fig. 2; and (Sec. C) a presentation of the theoretical model to estimate Landé g factor of the electron pockets, which includes Refs. [3–6].
- [3] R. Brown, R. Hartman, and S. Koenig, Tilt of the electron Fermi surface in Bi, *Phys. Rev.* **172**, 598 (1968).
- [4] P. Blaha, K. Schwarz, F. Tran, R. Laskowski, G. Madsen, and L. Marks, WIEN2k: An APW+lo program for calculating the properties of solids, *J. Chem. Phys.* **152**, 074101 (2020).
- [5] P. Giannozzi, S. Baroni, N. Bonini, M. Calandra, R. Car, C. Cavazzoni, D. Ceresoli, G. Chiarotti, M. Cococcioni, I. Dabo, A. Corso, S. Gironcoli, S. Fabris, G. Fratesi, R. Gebauer, U. Gerstmann, C. Gougoussis, A. Kokalj, M. Lazzeri, L. Martin-Samos *et al.*, QUANTUM ESPRESSO: a modular and open-source software project for quantum simulations of materials, *J. Phys.: Condens. Matter* **21**, 395502 (2009).
- [6] M. Kawamura, FermiSurfer: Fermi-surface viewer providing multiple representation schemes, *Comput. Phys. Commun.* **239**, 197 (2019).
- [7] O. Prakash, A. Kumar, A. Thamizhavel, and S. Ramakrishnan, Evidence for bulk superconductivity in pure bismuth single crystals at ambient pressure, *Science* **355**, 52 (2017).
- [8] Z. Zhu, B. Fauqué, Y. Fuseya, and K. Behnia, Angle-resolved Landau spectrum of electrons and holes in bismuth, *Phys. Rev. B* **84**, 115137 (2011).
- [9] H. Naren, R. Sannabhadti, A. Kumar, V. Arolkar, and S. Ramakrishnan, Setting up of a MicroKelvin refrigerator facility at TIFR, *AIP Conf. Proc.* **1447**, 503 (2012).
- [10] H. Fukuyama and R. Kubo, Interband effects on magnetic Susceptibility. II. Diamagnetism of bismuth, *J. Phys. Soc. Jpn.* **28**, 570 (1970).
- [11] J. Ruhman and P. Lee, Pairing from dynamically screened Coulomb repulsion in bismuth, *Phys. Rev. B* **96**, 235107 (2017).
- [12] M. Tinkham, *Introduction to Superconductivity* (Dover, New York, 1996).
- [13] P. Wolff, Matrix elements and selection rules for the two-band model of bismuth, *J. Phys. Chem. Solids* **25**, 1057 (1964).
- [14] S. Srinivasan, P. Bhattacharyya, and S. Jha, Superconducting transition temperature for semimetals like bismuth, *Pramana* **13**, 131 (1979).
- [15] Z. Mata-Pinzón, A. A. Valladares, R. M. Valladares, and A. Valladares, Superconductivity in bismuth. A new look at an old problem, *PLoS ONE* **11**, e0147645 (2016).
- [16] A. Migdal, Interaction between electrons and lattice vibrations in a normal metal, *Zh. Eksp. Teor. Fiz.* **34**, 1438 (1958) [*Sov. Phys. JETP* **7**, 966 (1958)].
- [17] S. Koley, M. Laad, and A. Taraphder, Dramatically enhanced superconductivity in elemental bismuth from excitonic fluctuation exchange, *Sci. Rep.* **7**, 10993 (2017)
- [18] G. Baskaran, Theory of ultra low T_c superconductivity in bismuth: Tip of an iceberg? *Physica C Supercond.* **552**, 48 (2018).
- [19] S. Tewari and C. Kapoor, Non-phononic mechanism of superconductivity in pure semi-metallic bismuth single crystal at sub-milli Kelvin, *Phys. Lett. A* **382**, 3131 (2018).
- [20] E. Krüger, Constraining forces stabilizing superconductivity in bismuth, *Symmetry* **10**, 44 (2018).